REGULAR PAPER

A Study on Laser Welding for Dissimilar Metals of Aluminum and Copper Using Pulsed Fiber Laser

Lanh Trinh[1] · Dongkyoung Lee[2,3,4]

Abstract

Joining dissimilar metals poses critical challenges due to differences in their properties, leading to the formation of brittle intermetallic compounds (IMCs). Aluminum (Al) and copper (Cu) are widely used in electrical applications for their advantageous characteristics. In lithium-ion batteries, joints of these metals aim to harness their physical and electrical beneficial features. However, aluminum and copper's high reflectivity and heat sensitivity present significant challenges in the joining processes. In the present study, a pulsed fiber laser, tailored for heat-sensitive components, was employed to weld Al/Cu and Cu/Al overlap configurations separately. Varied laser power ranges were applied to each welding configuration. The quality of the welds was assessed based on microstructure and mechanical properties. The results revealed the growth of dendritic IMCs towards the Al side in both welding configurations. Notably, the Al/Cu weld exhibited superior connection strength and fewer imperfections compared to the Cu/Al weld.

Keywords Laser welding · Dissimilar metals · Aluminum · Copper, microstructure, mechanical properties

1 Introduction

Lithium-ion batteries, vital components of electronic devices and electric vehicles, have garnered worldwide attention [1–3]. In response to global demand, manufacturers are actively enhancing battery performance, focusing on safety, durability, and power efficiency. The production of lithium-ion batteries involves multiple welding processes [4, 5], where the welded quality significantly impacts electrical flow and, subsequently, battery performance.

In the battery industry, aluminum (Al) and copper (Cu) are extensively used due to their excellent electrical conductivity. Besides, Al is recognized for its lightweight and malleable nature, while Cu boasts excellent tensile strength. The combination of these materials offers substantial benefits for enhancing battery performance. However, joining these dissimilar metals presents unique challenges, primarily stemming from the unforeseen formation of the brittle intermetallic compounds (IMCs) [6–8]. The formation of IMCs in the dissimilar weld of Al and Cu arises from the metal's low mutual solubility. The phase diagram of Al and Cu, depicted in Fig. 1, illustrates that the maximum solubility of Cu in Al is 2.5 at.%, and Al in Cu is about 19.7 at.%. Consequently, the nucleation of brittle Al-Cu IMCs can be favored during the solidification process when exceeding the solubility limit. These IMCs are generally brittle [9]. The growth of IMCs leads to a significant deterioration in weld properties giving rise to weld defects such as porosities and cracks [10, 11]. Additionally, an increase in IMCs thickness substantially elevates the contact resistance of Al-Cu joints [12]. Moreover, the distinct physical and metallurgical properties of the metals, including density, melting point, boiling point, and thermal conductivity, shown in Table 1, further complicate the joining of Al and Cu.

In recent years, various joining techniques have been proposed for Al-Cu joints, encompassing solid-state and fusion welding [8, 13]. Among these, friction-stir welding has

✉ Dongkyoung Lee
    ldkkinka@kongju.ac.kr

1   Department of Mechanical and Materials Engineering, University of Nebraska-Lincoln, Lincoln, NE 68588, USA

2   Department of Future Convergence Engineering, Cheonan College of Engineering, Kongju National University, Cheonan 31080, South Korea

3   Department of Mechanical and Automotive Engineering, Kongju National University, Cheonan 31080, South Korea

4   Center for Advanced Powder Materials and Parts of Powder (CAMP2), Kongju National University, Cheonan 31080, South Korea
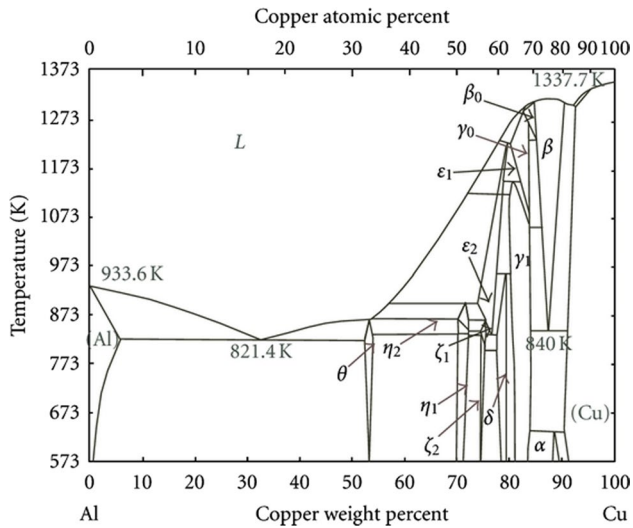
🙋 Springer KSPE

Fig. 1 The Al–Cu phase diagram according to Murray [36]

Table 1 Thermophysical properties of Al and Cu [37]

Material	Density (g/cm^3)	Melting point (°C)	Boiling point (°C)	Thermal conductivity (W/m K)
Aluminum	2.7	660	2470	205
Copper	8.96	1085	2562	385

garnered attention for its potential to join dissimilar metals like Al and Cu, as investigated in literature [14–16]. However, challenges associated with friction-stir welding have been reported, such as tool-related issues [17], and failures at the interface or nugget zone during mechanical testing [18, 19]. Ultrasonic spot welding, recognized for its energy efficiency and short weld time, has also been utilized for Al and Cu welding [20, 21]. Nevertheless, the methods have revealed issues, particularly related to tool matters, such as wear and tool-material contact, adversely affecting weld quality [22]. The feasibility of dissimilar joining for Al and Cu using resistance spot welding was also investigated [23], but studies also highlighted limitations, including materials, welding configuration, and tools. Thus, there exists a necessity for the development of a tool-free welding approach.

In recent developments, researchers and manufacturers have increasingly utilized laser beams in manufacturing processes [24–26] including welding for various materials [27]. Laser beam welding (LBW) offers unique features such as non-contact processing, high energy intensity, and ease of controlling energy input. LBW has successfully joined both similar and dissimilar thermal plastic materials [27–30]. Notably, LBW for dissimilar metals of Al and Cu has been investigated by many researchers. For instance, Xue et al.

[31] used ANSYS FLUENT to create a 3D finite volume simulation for the molten pool behavior for the weld of dissimilar metals of Al and Cu using a continuous wave laser source. The study concluded that an extensive interdiffusion of Cu and Al took place in the molten state with the given welding condition. Thus, different varieties of Al-Cu IMCs were formed in the weld. Dimatteo et al. [32] have developed laser welding for Al and Cu with a continuous-wave laser source using a beam oscillation technique, significantly improving weld quality. Wang et al. [33] explored an advanced welding technique using laser shock welding with a laser spot size of 6000 μm, demonstrating its feasibility in joining the dissimilar metals of Al and Cu with a nearly flat interface in the weld. Additionally, Zuo et al. [10] and Lerra et al. [34] performed laser for Al and Cu with different laser spot sizes. While most studies focus on continuous-wave lasers with a spot size in the hundreds of micrometers, there is less investigation into dissimilar Al and Cu joints using a pulsed wave laser with a focused spot size. Compared to continuous-wave lasers, pulsed wave lasers produce peak power for each pulse, allowing for deep penetration with a shorter interaction time, making them suitable for heat-sensitive components and reflective materials like Al and Cu [35].

In this study, we aim to investigate welding dissimilar Al and Cu using a pulsed wave laser beam with a focused spot size of 40 μ m. We compare two opposite lap welding configurations (Al/Cu and Cu/Al) focusing our analysis on microstructure characteristics and mechanical properties. The microstructure will be examined through cross-section observation, while mechanical properties, including hardness distribution and mechanical strength, will be thoroughly evaluated.

2 Experiment

Figure 2 depicts the schematic of the experimental setup, which employs an ytterbium pulsed fiber laser (IPG-YLPM, IPG photonics, Southbridge, Massachusetts USA) as the laser source. The laser's specifications are detailed in Table 2. Welding experiments with pure aluminum (Al, > 99.5%) and copper (Cu, > 99.5%) feature two overlap configurations: Al/Cu and Cu/Al. Due to the difference in laser absorbance of Al and Cu, a single set of laser parameters is not feasible for both welding configurations. Therefore, the laser power varies based on the configuration, as determined through preliminary experiments. This variation ensures optimal weldability, starting from the minimum power required for effective material joining. The laser power variations for each configuration are outlined in Table 3.
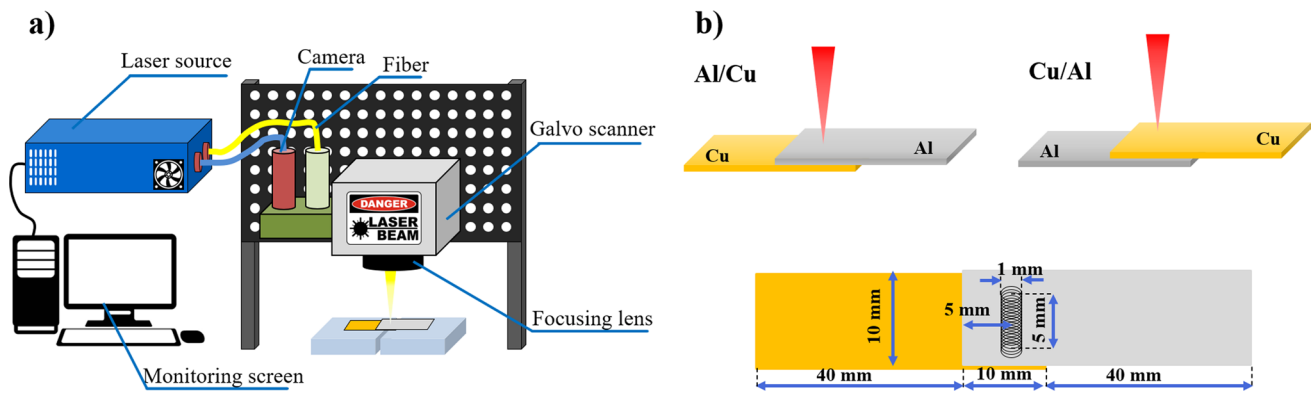
Fig. 2 **a** Schematic of the experimental setup, **b** Welding configurations

Table 2 Specifications of the laser source

Laser type	Pulsed fiber laser
Maximum laser power	300 W
Wavelength	1064 nm
Pulse duration	20 ns
Spot size	40 µm
Frequency	2000 kHz

Table 3 Laser power and wobbling specification

Configuration	Laser power range (W)	Wobbling	
		Amplitude (mm)	Frequency (kHz)
Al/Cu	80–160	0.5	100
Cu/Al	180–260		

Additionally, the study employs the wobbling technique, previously proven to enhance weld quality [30, 32]. The materials used are Al and Cu sheets, with thicknesses of 0.27 mm and 0.3 mm respectively, serving as welding specimens. The welds are executed in an overlap configuration, as illustrated in Fig. 2b).

The examination of the welded specimen commences with a Dino-lite microscope, capturing both top and bottom views. This is followed by a detailed microstructure analysis using a scanning electron microscope (SEM) equipped with an energy-dispersive X-ray spectroscopy (EDX) detector (Mira CMH, TESCAN, Brno, Czech Republic) to scrutinize the weld's microstructure and chemical composition in cross-section. To identify mechanical properties, Vickers microhardness measurements along the cross-section of the weld are performed with a Mitutoyo HM-100 series microhardness machine, using a load of 0.49 N for a dwell time of 10 s. Additionally, the shear strength of the joint is measured using a universal testing machine (Shimadzu Ag–X Plus, Shimadzu

Europa GmbH, Duisburg, Germany) with a loading speed of 0.5 mm/min.

3 Result and Discussion

3.1 Microstructure

The morphology of the top and bottom surfaces of the weld in both configurations is examined and shown in Fig. 3. In the weld of Al/Cu, the top surface exhibits a clean weld appearance without visible spatters. Conversely, a noticeable heat-affected zone tends to enlarge at the end of the welding line in the Cu/Al weld. When observing from the bottom, evidence of heat-affected evidence is visible from the laser power of 120 W when Al is on top of Cu. Meanwhile, in the Cu/Al weld, full penetration can be observed from the laser power of 180 W. Overall, as the laser power increases, there is a growth in visible defects on the bottom view, indicating an increase in penetration.

Figure 4 exhibits the cross-section view in Al/Cu and Cu/Al joints. In Al/Cu, an increased laser power correlates with enhanced penetration depth. Pores appear at 140 W and 160 W mainly in the upper material (Al). At 140 W, the porosities align with the interface, while at 160 W, pores form around visible cracks initiated from the Al material. It is important to note that most of the pores formed in the Al/Cu weld have spherical shape indicating their origin of gas entrapment. While pores are almost free at the low laser power (80 W and 100 W) where the penetration to the Cu layer is limited. Nevertheless, Al is bonded to Cu indicating the interdiffusion at the interface due to heat conduction from surface melted Al. An increasing laser power leads to deeper penetration into Cu layer together with more pore formation. Notably, these pores are primarily located within the Al layer, although the penetration is apparently deep into Cu layer. In the keyhole welding mode, the instability and collapse of
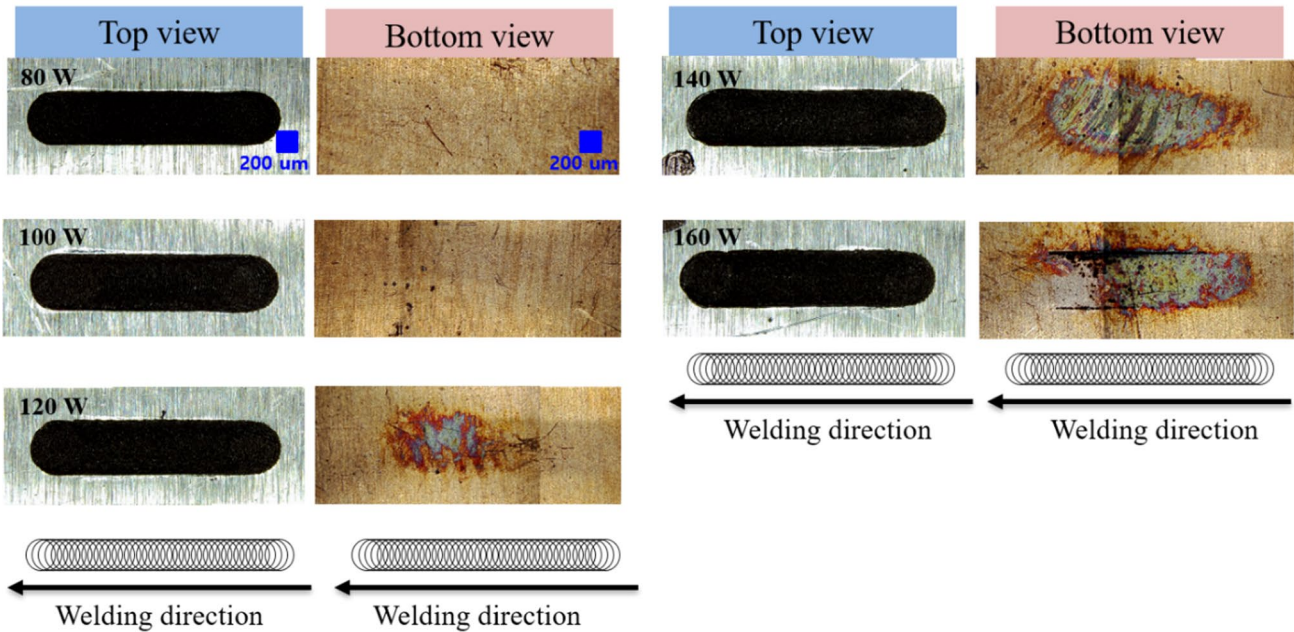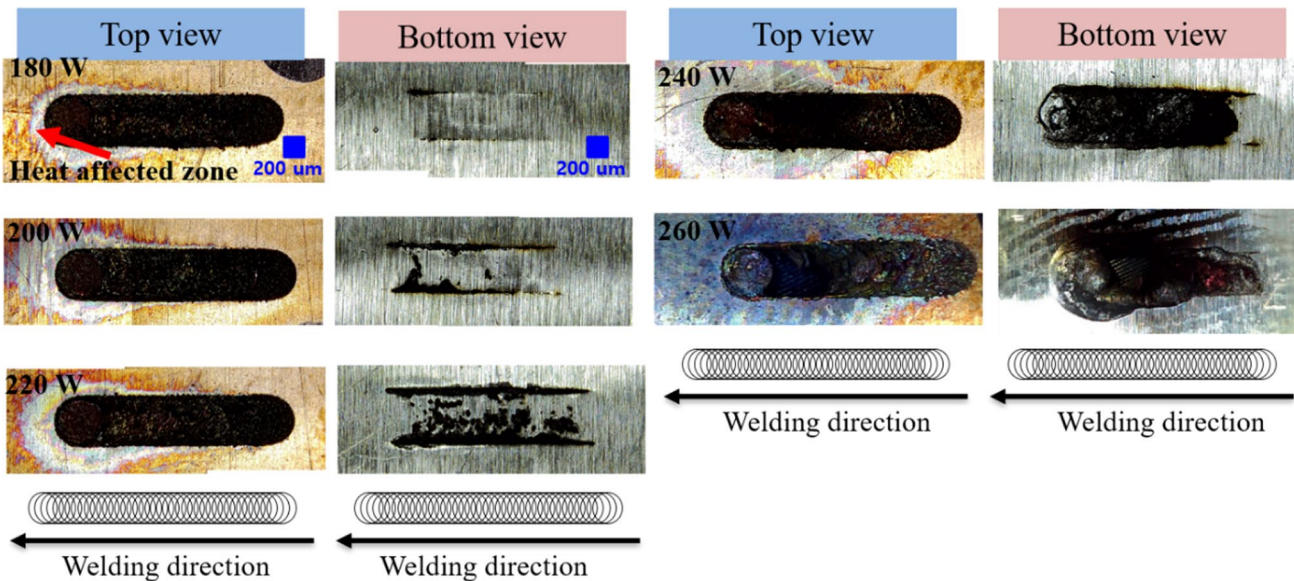
Fig. 3 Top view and bottom view of the weld **a** Al/Cu, **b** Cu/Al

the keyhole are the major sources of gas entrapment, in turn leading to the spherical pore formation at the bottom of the keyhole. In this study, the pores remain within the Al layer although the laser readily penetrates the Cu layer, indicating the instability of the keyhole within the Al layer. The high reflectance of Cu [38] is assumed to result in multiple scattering as the laser reaches the Cu layer. Consequently, the keyhole in the melt pool becomes

significantly unstable, leaving pores behind as the laser scanned through. Moreover, cracks are readily observed in the sample after solidification at 180W, indicating a crack-sensitive phase and solidification-induced stress formed during solidification. In contrast, the Cu/Al weld exhibits a fluctuating weld surface with significant material loss, increasing with laser powers. As mentioned above, the high reflectance of Cu results in scattering of the laser
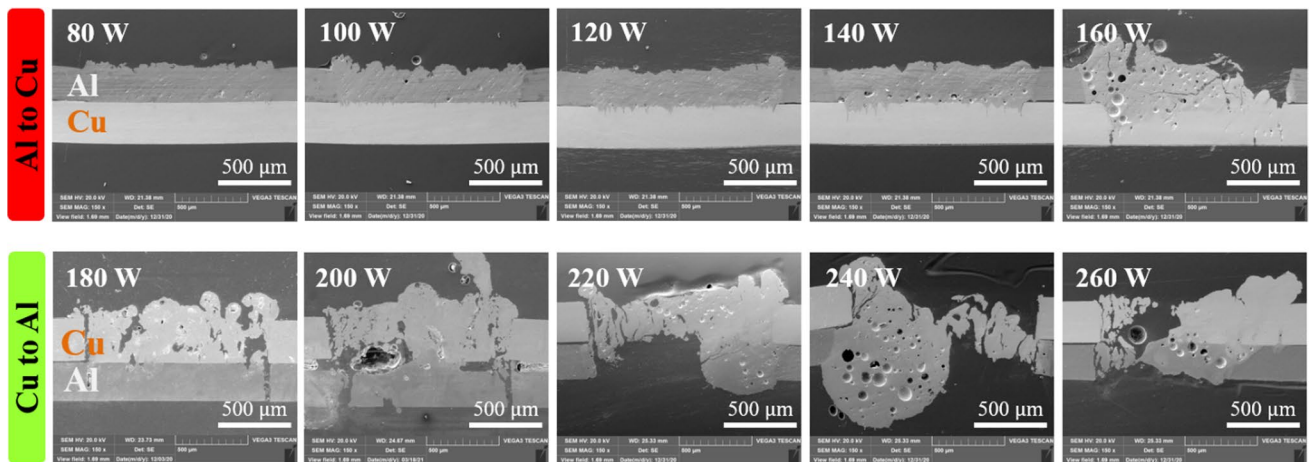
Fig. 4 Cross-section views the weld of Al/Cu and Cu/Al

beam. Associating with high energy input, ablation of Cu can occur readily leading to the loss of material. Besides, pores are abundant in Cu/Al weld.

The microstructure in both welds, as shown in Fig. 5, exhibits a dendritic structure expanding towards the Al side. Moreover, Cu islands, where the dendritic structure originates from, formed within Al layer. The formation of the dendritic structure indicates a rapid cooling of the molten materials, leading to a high velocity of the liquid–solid interface and a high undercooling with the Al melt pool. At these conditions, the solid–liquid interface becomes unstable and breaks down leading to the protrusion growth of the dendritic structure. Beyond the dendritic layer, an intermediate layer formed before reaching the eutectic microstructure and Al side. The analysis of the phases presented in this region requires extensive characterization techniques. For the sake of this study, the analysis of the microstructure of the interface region focuses on the morphology of the phase presented. Further studies will focus on the nature of the phases and their impact on the mechanical properties

Fig. 5 Microstructure at the interface of the weld *a* Al/Cu, **b** Cu/Al
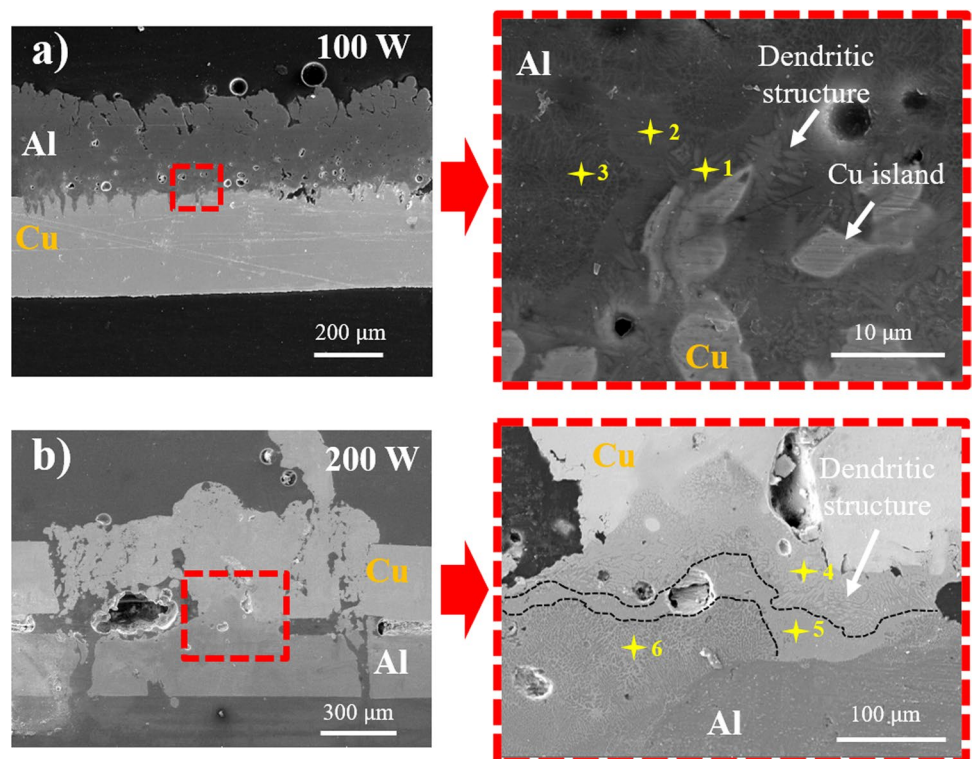
Table 4 Chemical composition on the cross-section of the points in Fig. 5

Point	Al (at%)	Cu (at%)	Possible phase
1	61.16	38.84	Al_2Cu
2	83.88	16.12	Al+IMCs
3	87.52	12.48	Al+IMCs
4	69.86	30.14	Al_2Cu
5	83.65	16.35	Al+IMCs
6	89.55	10.45	Al+IMCs
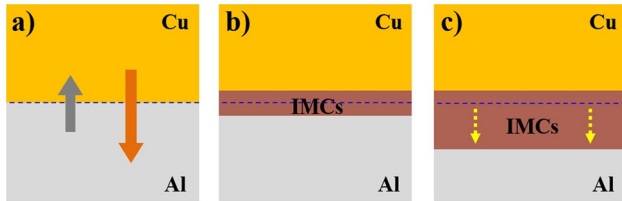
Fig. 6 Kirkendall effect **a** Diffusion of Al and Cu, **b** IMCs formation, **c** IMCs expansion

of the joint. However, it is important to note that the presence of the multiphase with the interface region introduces more interface boundaries which in turn act as a barrier for dislocations motion, strengthening the joints. However, the nature of the phase is significant to the strengthening effect. For instance, some brittle IMCs contain limited slip systems, where dislocation motions can occur to accommodate the deformation. Thus, they become brittle and are prone to initiate cracks and deteriorate the weld. EDS analysis of chemical composition in the dendritic structure has been examined and shown in Table 4. Given the EDS results, possible phases in the interface region including IMCs phases

are presented. Meanwhile, a thicker layer of dendritic structure can be observed in the case of Al on top in comparison with the weld of Cu/Al. A reliable explanation for the expansion of dendritic structure into the Al side relates to the phenomenon of the Kirkendall effect which is demonstrated by Smigelskas and Kirkendall [39]. The Kirkendall effect illustrates the interface motion between metals due to differences in diffusion rates. The illustration of the effect is indicated in Fig. 6. During the welding process, the atoms of Al and Cu start to diffuse to each other. The diffusion rate of Cu is generally five times higher than that of Al, and the diffusion rate of Cu is linearly proportional to temperature (a) [40]. During welding, Al and Cu atoms diffuse, with Cu having a faster rate. Interdiffusion leads to the formation of Al-Cu IMCs (b). Due to Al's lower diffusion rate, the spread of IMCs tends to favor the Al side (c).

3.2 Mechanical Properties

3.2.1 Microhardness

Vickers hardness measurement is conducted vertically in the cross-section of the weld from the upper material to the lower material. The hardness measurement of the weld of Al/Cu is presented in Fig. 7. Within the upper material (Al) in the Al/Cu weld, hardness increases as the distance gets closer to the interface. At 80 W, up to a distance of 100 μm from the Al surface, the hardness distribution remains similar to the base materials (Al: 60 HV, Cu: 117 HV). At 100 W, a sharp increase in hardness occurs at the interface. When the laser powers of 120 W, 140 W, and 160 W are used, a significant rise in hardness happens at the distance of 50 μ*m* from the interface. Generally, the peak hardness at each laser power increases and shifts towards the Al side with increasing laser power. In particular, the maximum hardness at the

Fig. 7 Hardness distribution in the weld of Al/Cu
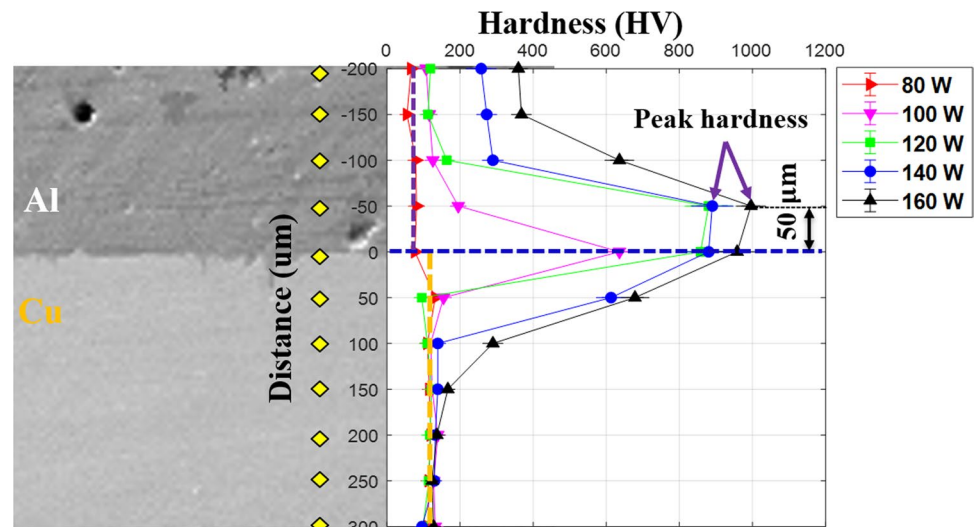
laser power of 100 W and 120 W are 625.9 HV and 880 HV, respectively. Meanwhile, the peak hardness obtained at the laser power of 140 W is 890 HV, and at the laser power of 160 W is 995.7 HV. In the lower material (Cu), the hardness decreases significantly at the distance of 50 µm and 100 µm from the interface. From the distance of 150 µm towards the bottom, there is an insignificant variation of the hardness among different laser powers. The slight hardness increase within approximately 100 µm from the Al surface is attributed to the recrystallization of the Al after melting by laser irradiation. High energy input together with fast solidification gives rise to the driving force for the nucleation of liquid Al. The higher laser power, the higher energy input to melt the Al. As a result, the temperature in liquid Al increases, which in turn increases the undercooling and amount of nucleation event during solidification. Consequently, the microstructure (i.e., grain size) is refined. Thus, the hardness increases as laser power increases. However, the shape rise in hardness near the interface correlates with the presence of intermediate phases (IMCs) due to the interdiffusion of Al and Cu at this region.

Figure 8 indicates the hardness profile of the weld with Cu on top of Al. Overall, the material surrounding the interface is reported with high hardness. Within the upper material (Cu) at all laser powers, hardness increases as the distance is close to the interface. Peak hardness values at the laser power of 180 W and 200 W are measured at the interface of Al and Cu. Meanwhile, the maximum hardness values at the laser power of 220 W and 240 W are detected on the Al side at the distance of 50 µm and 100 µm from the interface, respectively. On the Al side, it is noticed that the high hardness zone expands together with the increase of the laser power. In particular, at the laser power of 200 W, the material with a hardness exceeding 300 HV remains till the distance of 50 µm from the interface. In comparison, at the laser power of 220 W and 240 W, the high hardness zone remains within the distances of 200 µm and 250 µm from the interface, respectively.

3.2.2 Mechanical Strength

The mechanical strength of the weld is assessed through a shear strength test, and Fig. 9 presents the ultimate loading forces of each weld at different laser powers. It is evident that the Al/Cu weld achieves higher strength compared to the Cu/Al weld. Furthermore, optimal laser power for the maximum mechanical strength is identified in both cases. Specifically, in the weld of Al/Cu, an average shear loading force of 246.82 N is attained at the laser power of 80 W. A loading force of 297.59 N, higher than the shear strength force of base Al (260 N) but lower than the base Cu (490 N), is recorded at 100 W. However, at 120 W, 140 W, and 160 W, the loading forces decrease, correlating with the increase in intermetallic compound (IMC) formation in the weld, as depicted in Fig. 10. The intermixture region of Al and Cu in the interface, where possible multiple brittle phases are present, of the weld Al/Cu increases with increasing laser power.

In the Cu/Al weld configuration, the shear strength exhibits a similar trend within the specified laser power range. At 180 W, the average ultimate loading force recorded is 64.85 N, increasing to 83.8 N at 200 W. Subsequently, the average force decreases with higher laser powers. The lowest weld strength is observed at 260 W, with an average load capacity of 57.64 N. Notably, the reduction in strength in Cu/Al welds is attributed to the loss of weld metal in the weld zone due to evaporation, as depicted in Fig. 4. The loss of the weld metal will weaken the connection strength.

Moreover, the fracture behavior of Al/Cu and Cu/Al welds are significantly different. Figure 11 demonstrates

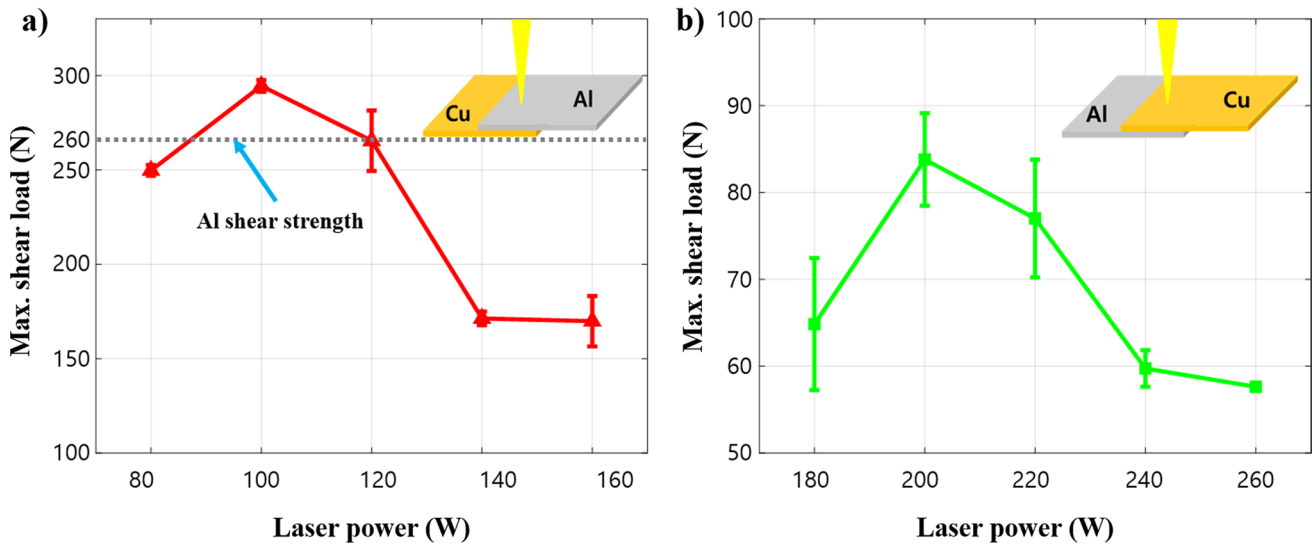**Fig. 8** Hardness distribution in the weld of Cu/Al
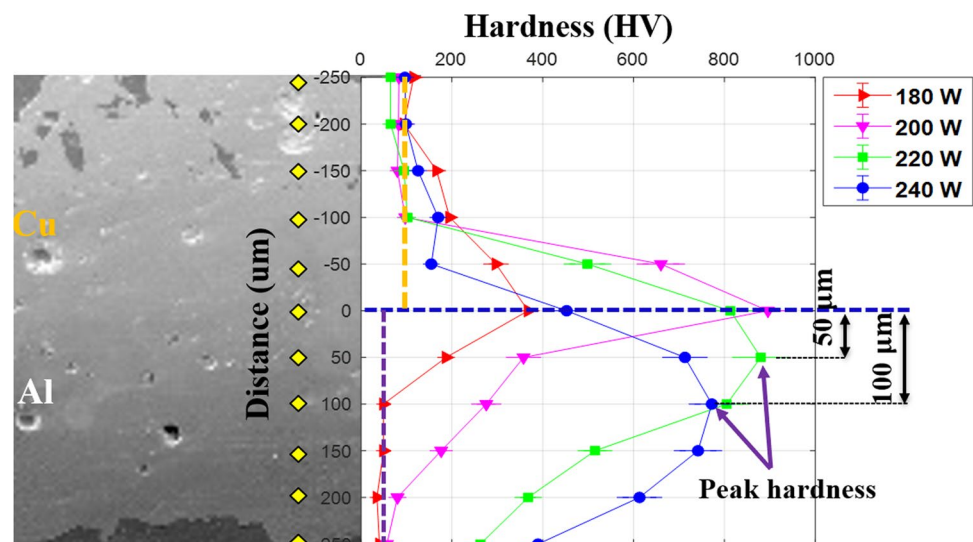
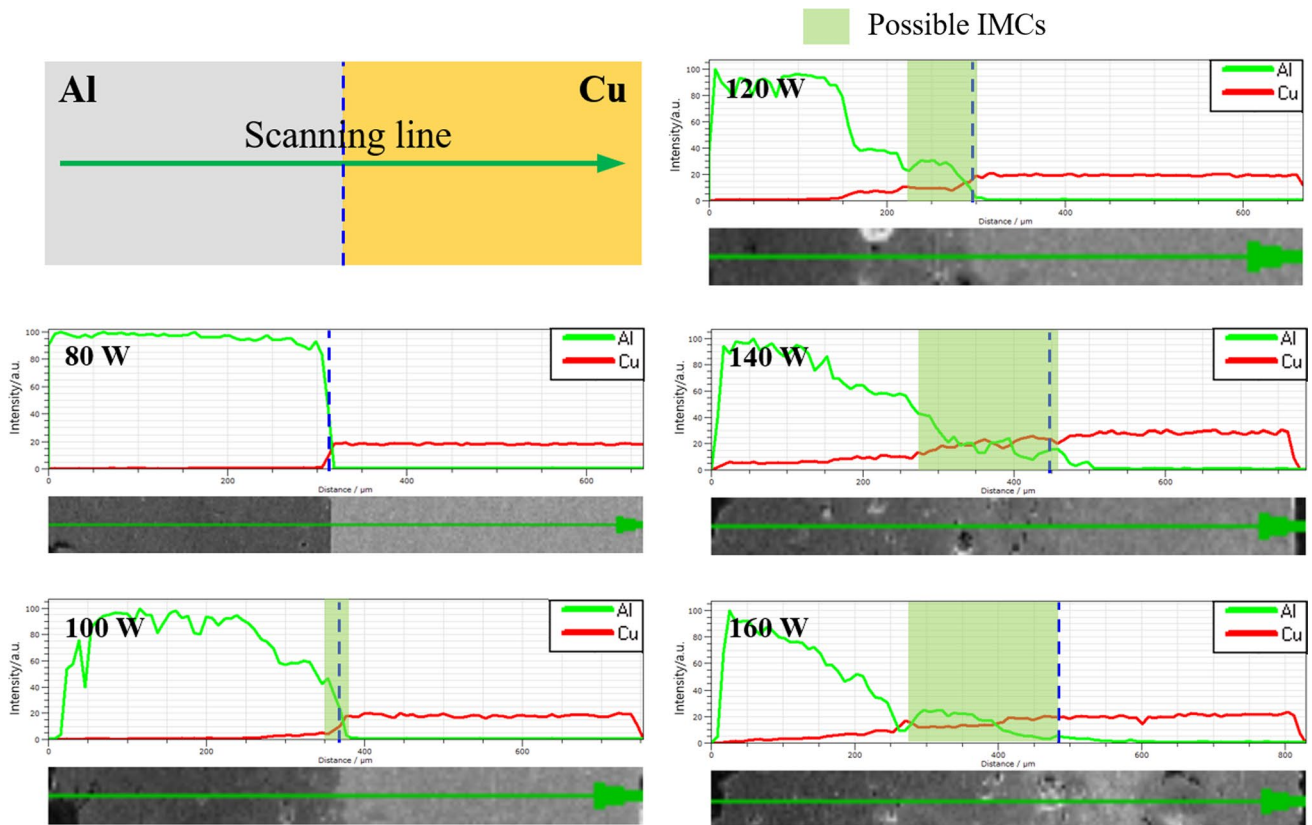**Fig. 9** Shear strength of the weld **a** Al/Cu, **b** Cu/Al

Fig. 10 EDS line scans through the interface of the weld of Al/Cu

the shear strength test result for the weld of Al/Cu and Cu/Al with the presence of elongation. Overall, the weld of Al/Cu results in a longer elongation before it fractures than the weld of Cu/Al. Moreover, the fracture of most of the weld in the configuration of Cu/Al happens at the ultimate load points, while there is elongation after the ultimate load in the case of the Al/Cu weld. In short, the weld of Al/Cu is more ductile than the weld of Cu/Al.
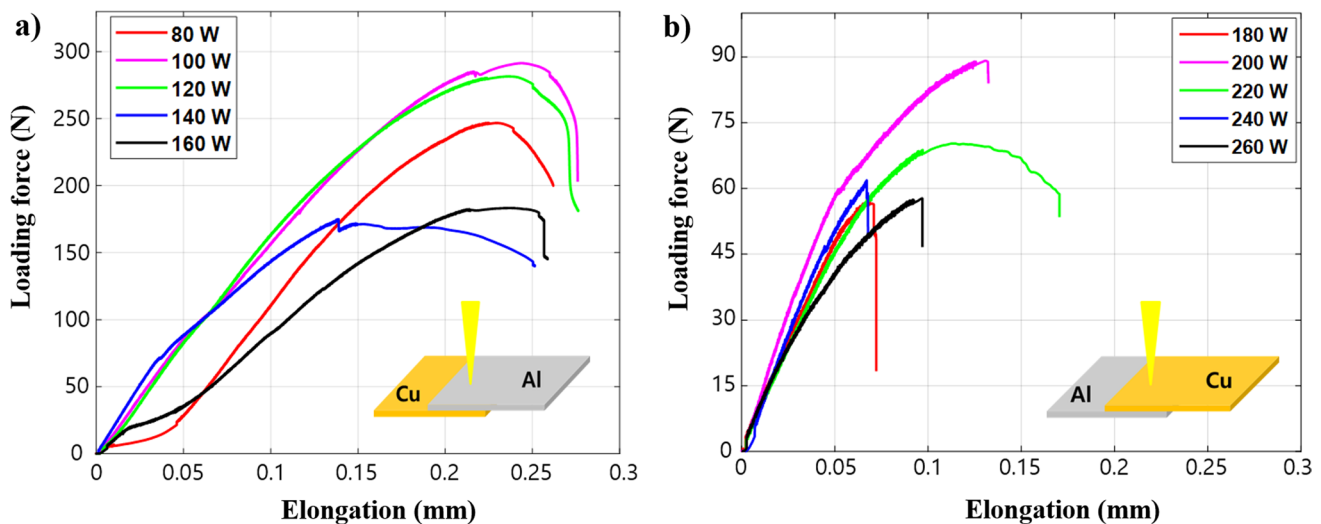
Fig. 11 Result of the shear strength test **a** Al/Cu, **b** Cu/Al

4 Conclusion

In this study, the welding of dissimilar metals, Al and Cu, is conducted using a pulsed fiber laser. The application of a pulsed wave laser provides many benefits for joining heat-sensitive components, thanks to the concentrated laser beam and short pulse duration which leads to less interaction time. The evaluation of the welding results encompasses microstructure observation and mechanical behavior. Notably, the Al/Cu weld demands lower laser energy for successful welding, and when Al is positioned on top, it exhibits notable favorable characteristics compared to the Cu/Al weld. Several conclusions can be drawn as follows:

- The formation of IMCs with dendritic structure expands towards Al in both cases of Al on top and Cu on top. This occurs due to the solubility limit and differences in the diffusion rate of the base metals explained by the Kirkendall effect.
- The weld metal on the Al side is obtained with higher hardness than that on the Cu side. Cu/Al weld manifests a deeper extension of high-hardness weld metal on the Al side than Al/Cu weld.
- Under the given welding conditions, the highest shear strength for Al/Cu and Cu/Al welds is achieved at laser powers of 100 W and 200 W, respectively. Additionally, Al/Cu weld demonstrates superior strength and ductility compared to Cu/Al weld.

While pulsed wave laser technology delivers high peak laser power with each pulse, enabling deep penetration of the laser into the materials. This often results in the formation of a keyhole in the melt. The keyhole's instability, caused by the multi-scale reflection of the laser beam, can lead to the formation of pores as the keyhole collapses. Additionally, thermal stress from rapid cooling of the melt pool can induce cracks. To address these issues, one potential solution is to reduce the reflectance of Al and Cu under laser irradiation or increase their absorbance, which can be achieved using blue or green lasers. Enhanced laser absorption allows the materials to absorb more photon energy, converting it into heat to facilitate melting and accelerate diffusion. This strengthens the joint by improving materials interdiffusion while mitigating keyhole formation. Surface modification techniques such as surface alloying or plating with elements exhibiting high near-infrared laser absorption (e.g., Fe) could enhance the laser absorption of the base Cu and Al. Furthermore, given the ultrahigh absorption rates of Cu and Al in the blue and green wavelength bands, utilizing lasers within these bands could be advantageous. Conversely, preheating proves effective in reducing the cooling rate of the melt pool, thereby preventing crack formation due to thermal stress. These discussions warrant further investigation into laser beam welding of highly reflective materials such as Al and Cu.

Declarations

Conflict of interest On behalf of all authors, the corresponding author states that there is no conflict of interest.

References

1. Yuan, X., & Wu, J. (2020). Research on the development of pure electric vehicle power battery technology based on patent analysis. *IOP Conference Series: Earth and Environmental Science.* https://doi.org/10.1088/1755-1315/615/1/012081

2. Manthiram, A. (2017). An outlook on lithium ion battery technology. *ACS Central Science, 3*(10), 1063–1069. https://doi.org/10.1021/acscentsci.7b00288

3. Zubi, G., Dufo-López, R., Carvalho, M., & Pasaoglu, G. (2018). The lithium-ion battery: State of the art and future perspectives. *Renewable and Sustainable Energy Reviews, 89*, 292–308. https://doi.org/10.1016/j.rser.2018.03.002

4. Lee, S. S., Kim, T. H., Hu, S. J., Arbor, A., Cai, W. W., & Abell, J. A. (2016). Joining technologies for automotive Li-ion battery manufacturing—A review (pp. 1–9).

5. Trinh, L. N., & Lee, D. (2020). Welding of thin tab and battery case for lithium-ion battery cylindrical cell using nanosecond pulsed fiber laser. *Journal of Welding and Joining, 38*(4), 389–394. https://doi.org/10.5781/jwj.2020.38.4.8

6. Hannech, E. B., Lamoudi, N., Benslim, N., & Makhloufi, B. (2003). Intermetallic formation in the aluminum-copper system. *Surface Review and Letters, 10*(4), 677–683. https://doi.org/10.1142/S0218625X03005396

7. Abbasi, M., Karimi Taheri, A., & Salehi, M. T. (2001). Growth rate of intermetallic compounds in Al/Cu bimetal produced by cold roll welding process. *Journal of Alloys and Compounds, 319*(1–2), 233–241. https://doi.org/10.1016/S0925-8388(01)00872-6

8. Chatterjee, S., Trinh, L. N., & Lee, D. (2022). Mechanical and microstructural investigation of dissimilar joints of Al-Cu and Cu-Al metals using nanosecond laser. *Journal of Mechanical Science and Technology, 36*(8), 4205–4211. https://doi.org/10.1007/S12206-022-0738-X

9. Hug, E., & Bellido, N. (2011). Brittleness study of intermetallic (Cu, Al) layers in copper-clad aluminium thin wires. *Materials Science and Engineering A, 528*(22–23), 7103–7106. https://doi.org/10.1016/j.msea.2011.05.077

10. Zuo, D., Hu, S., Shen, J., & Xue, Z. (2014). Intermediate layer characterization and fracture behavior of laser-welded copper/aluminum metal joints. *Materials and Design, 58*, 357–362. https://doi.org/10.1016/j.matdes.2014.02.004

11. Du, H., Shin, J. H., & Lee, S. W. (2005). Study on porosity of plasma-sprayed coatings by digital image analysis method. *Journal of Thermal Spray Technology, 14*(4), 453–461. https://doi.org/10.1361/105996305X76450

12. Braunovid, M., & Aleksandrov, N. (1992). Intermetallic compounds at aluminum-to-copper and copper-to-tin electrical interfaces. In *Proceedings of the thirty-eighth IEEE Holm conference on electrical contacts, vol. 1992,* October (pp. 25–34). https://doi.org/10.1109/HOLM.1992.246938.

13. Bui-Thi, T. A., Do, T. T., Zhang, S., Kim, Y., Han, H. N., & Hong, S. T. (2024). Comparative study of electrically assisted pressure joining of aluminum 6061–T6 alloys and copper C11000 alloys. *International Journal of Precision Engineering and Manufacturing - Green Technology, 11*(3), 877–888. https://doi.org/10.1007/S40684-024-00617-9/FIGURES/11

14. Akinlabi, E. T., Andrews, A., & Akinlabi, S. A. (2014). Effects of processing parameters on corrosion properties of dissimilar friction stir welds of aluminium and copper. *Transactions of Nonferrous Metals Society of China, 24*(5), 1323–1330. https://doi.org/10.1016/S1003-6326(14)63195-2

15. Xue, P., Ni, D. R., Wang, D., Xiao, B. L., & Ma, Z. Y. (2011). Effect of friction stir welding parameters on the microstructure and mechanical properties of the dissimilar Al-Cu joints. *Materials Science and Engineering A, 528*(13–14), 4683–4689. https://doi.org/10.1016/j.msea.2011.02.067

16. Ouyang, J., Yarrapareddy, E., & Kovacevic, R. (2006). Microstructural evolution in the friction stir welded 6061 aluminum alloy (T6-temper condition) to copper. *Journal of Materials Processing Technology, 172*(1), 110–122. https://doi.org/10.1016/j.jmatprotec.2005.09.013

17. Mehta, K. P., & Badheka, V. J. (2016). A review on dissimilar friction stir welding of copper to aluminum: Process, properties, and variants. *Materials and Manufacturing Processes, 31*(3), 233–254. https://doi.org/10.1080/10426914.2015.1025971

18. Ouyang, J. H., & Kovacevic, R. (2002). Material flow and microstructure in the friction stir butt welds of the same and dissimilar aluminum alloys. *Journal of Materials Engineering and Performance, 11*(1), 51–63. https://doi.org/10.1007/s11665-002-0008-0

19. Murr, L. E., Flores, R. D., Flores, O. V., McClure, J. C., Liu, G., & Brown, D. (1998). Friction-stir welding: Microstructural characterization. *Materials Research Innovations, 1*(4), 211–223. https://doi.org/10.1007/s100190050043

20. Kumar, N. A. P. K., Li, C., Leonard, K. J., Bei, H., & Zinkle, S. J. (2016). Microstructural stability and mechanical behavior of FeNiMnCr high entropy alloy under ion irradiation. *Acta Materialia, 113*, 230–244. https://doi.org/10.1016/J.ACTAMAT.2016.05.007

21. Zhang, Z., Wang, K., Li, J., Yu, Q., & Cai, W. (2017). Investigation of interfacial layer for ultrasonic spot welded aluminum to copper joints. *Science and Reports, 7*(1), 1–6. https://doi.org/10.1038/s41598-017-12164-2

22. Ni, Z. L., et al. (2020). Ultrasonic spot welding of aluminum to copper: A review. *International Journal of Advanced Manufacturing Technology, 107*(1–2), 585–606. https://doi.org/10.1007/s00170-020-04997-5

23. Zhang, Y., et al. (2016). Feasibility study of dissimilar joining of aluminum alloy 5052 to pure copper via thermo-compensated resistance spot welding. *Materials and Design, 106*(June), 235–246. https://doi.org/10.1016/j.matdes.2016.05.117

24. Seo, Y., Trinh, L. N., & Lee, D. (2023). The influence of the proportion of silica sand on cement mortar during laser irradiation. *Materials Chemistry and Physics, 296*, 127253. https://doi.org/10.1016/J.MATCHEMPHYS.2022.127253

25. Trinh, L., et al. (2024). Transmission electron microscopy characterizations of local amorphization of single crystal silicon by nanosecond pulsed laser direct writing. *Advanced Engineering Materials, 26*(2), 2301377. https://doi.org/10.1002/ADEM.202301377

26. Wang, X., et al. (2024). Direct observation and quantification of nanosecond laser induced amorphization inside silicon. *Journal of Laser Applications.* https://doi.org/10.2351/7.0001305

27. Sun, Z., & Ion, J. C. (1995). Laser welding of dissimilar metal combinations. *Journal of Materials Science, 30*(17), 4205–4214. https://doi.org/10.1007/BF00361499

28. Trinh, L. N., & Lee, D. (2020). The characteristics of laser welding of a thin aluminum tab and steel battery case for lithium-ion battery. *Metals, 10*(6), 842. https://doi.org/10.3390/MET10060842

29. Hong, K. M., & Shin, Y. C. (2017). Prospects of laser welding technology in the automotive industry: A review. *Journal of Materials Processing Technology, 245*, 46–69. https://doi.org/10.1016/j.jmatprotec.2017.02.008

30. Trinh, L., & Lee, D. (2024). Effect of welding path on the weld quality of aluminum tab and steel battery case in lithium-ion

battery. *Journal of Mechanical Science and Technology., 38*(5), 1–11. https://doi.org/10.1007/S12206-024-0417-1

31. Xue, Z., Hu, S., Zuo, D., Cai, W., Lee, D., & Elijah, K. A. (2013). Molten pool characterization of laser lap welded copper and aluminum. *Journal of Physics D: Applied Physics*. https://doi.org/10.1088/0022-3727/46/49/495501

32. Dimatteo, V., Ascari, A., & Fortunato, A. (2019). Continuous laser welding with spatial beam oscillation of dissimilar thin sheet materials (Al-Cu and Cu-Al): Process optimization and characterization. *Journal of Manufacturing Processes, 44*(June), 158–165. https://doi.org/10.1016/j.jmapro.2019.06.002

33. Wang, X., Gu, C., Zheng, Y., Shen, Z., & Liu, H. (2014). Laser shock welding of aluminum/aluminum and aluminum/copper plates. *Materials and Design, 56*, 26–30. https://doi.org/10.1016/j.matdes.2013.10.091

34. Lerra, F., Ascari, A., & Fortunato, A. (2019). The influence of laser pulse shape and separation distance on dissimilar welding of Al and Cu films. *Journal of Manufacturing Processes, 45*(April), 331–339. https://doi.org/10.1016/j.jmapro.2019.07.015

35. Trinh, L. N., & Lee, D. (2020). The effect of using a metal tube on laser welding of the battery case and the tab for lithium-ion battery. *Materials (Basel), 13*(19), 4460. https://doi.org/10.3390/ma13194460

36. Murray, J. L. (1985). The aluminium-copper. 30(5).

37. Committee, A. H. (1990). Properties and selection: Nonferrous alloys and special-purpose materials. *Properties and Selection: Nonferrous Alloys and Special-Purpose Materials*. https://doi.org/10.31399/ASM.HB.V02.9781627081627

38. Wang, B., & Gallais, L. (2013). A theoretical investigation of the laser damage threshold of metal multi-dielectric mirrors for high power ultrashort applications. *Optics Express, 21*(12), 14698. https://doi.org/10.1364/oe.21.014698

39. Nakajirna, H. (1997). The discovery and acceptance of the Kirkendall effect: The result of a short research career. *JOM Journal of the Minerals Metals and Materials Society, 49*(6), 15–19.

40. Mao, A., et al. (2020). The diffusion behaviors at the Cu-Al solid–liquid interface: A molecular dynamics study. *Results in Physics*. https://doi.org/10.1016/j.rinp.2020.102998

Lanh Trinh obtained his Master of Science in Mechanical Engineering from Kongju National University, Cheonan, Korea, in 2021. During his master's program, his research specialized in laser welding for dissimilar metals in Lithium-ion batteries including Aluminum and coppoer as well as Aluminum and stainless steel. Currently, he is pursuing a Ph.D. program in Materials Engineering at the University of Nebraska-Lincoln, NE, U.S.A. His current research focuses on advanced manufacturing and irradiation damage characterization in compositionally complex carbide materials tailored for extreme environments, encompassing high temperature, corrosion, and irradiation.
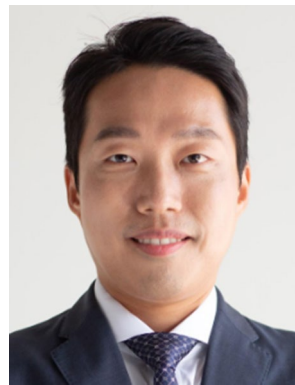
Dongkyoung Lee received his Ph.D. in Mechanical Engineering in 2012 and an M.S. degree in the same field in 2011, both from the University of Michigan, Ann Arbor, MI, U.S.A. He also earned an M.S. in Aerospace Engineering from the same university in 2017, and a B.S. degree in Mechanical Engineering from Hanyang University, Seoul, South Korea in 2006. Currently, he is an Associate (Tenured) Professor at Kongju National University, South Korea, in the Department of Mechanical and Automotive Engineering, Department of Future Convergence Engineering, and Center for Advanced Materials and Parts of Powder (CAMP2). His research focuses on laser-aided manufacturing, with particular emphasis on applications in lithium-ion batteries, fuel cells, nuclear decommissioning, advanced semiconductor packaging, and display technologies.